Ceramics International 49 (2023) 23287–23294

Contents lists available at ScienceDirect

Ceramics International

journal homepage: www.elsevier.com/locate/ceramint

Effect of hydrothermal time on the forming specific morphology of YPO_4:Eu^{3+} nanoparticles for dedicated luminescent applications as optical markers

Francesco Armetta [a,b], Vitalii Boiko [c], Dariusz Hreniak [c], Cecilia Mortalò [d], Cristina Leonelli [e], Ludovico Barbata [a], Maria Luisa Saladino [a,b,*]

[a] Department of Biological, Chemical and Pharmaceutical Sciences and Technologies (STEBICEF), University of Palermo and INSTM UdR – Palermo, Viale delle Scienze, Bld.17, Palermo, I-90128, Italy
[b] IPCF-CNR, Istituto per i Processi Chimico Fisici, V.le F. S. d'Alcontres 37, I-98158, Messina, Italy
[c] Institute of Low Temperature and Structure Research, Polish Academy of Sciences, Ul Okólna 2, Wrocław, Poland
[d] Institute of Condensed Matter Chemistry and Energy Technologies (ICMATE), National Research Council of Italy (CNR), C.so Stati Uniti 4, IT-35127, Padova, Italy
[e] Department of Engineering "Enzo Ferrari", University of Modena and Reggio Emilia, Via Pietro Vivarelli 10, IT-41125, Modena, Italy

ARTICLE INFO

Handling Editor: P. Vincenzini

Keywords:
Orthophosphates
Rare-earths
Particles shaping
Hydrothermal treatment
Water adsorption
Nano-needles
Luminescence

ABSTRACT

A way to control the desired shape and microstructure of YPO_4:Eu^{3+} nanoparticles through the precipitation method followed by a hydrothermal treatment is reported. This method is useful for achieving very high control over the YPO_4:Eu^{3+} formation process with the selection of appropriate synthesis parameters. In detail, the autoclave processing time allows control of the shape and size of nano-needle-shaped particles independently in both directions, as confirmed by X-ray powder diffraction, FT-IR Spectroscopy and Electron Transmission Microscopy. In order to analyse the effect of the nanoparticles' surroundings on the excitation and relaxation processes of luminescent ions, Eu^{3+} ion was used as a dopant, whose specific properties allow the study of changes in their local surroundings by analysing emission spectra. As additionally shown, the shape and size of the nano-needles were correlated with the luminescence properties of the particles, which are particularly influenced by the presence of water and by its effect on emission processes from dopant ions located in the near-surface zone of the nanoparticles. These results proved that the shape of particles influenced the distance between Eu^{3+} ions in the phosphor, such distance affected the specific emission properties, i.e. the lifetime of excited levels of Eu^{3+} ions.

1. Introduction

In principle, it is now impossible to imagine our world without all the benefits provided by inorganic luminescent materials. Intriguing for centuries and used since modern times, they now accompany us not only in the creation of suitable lighting, but also in almost every aspect of modern technology. These materials are now used in every form, from large-scale crystals, glasses and ceramics used to build high power lasers and supersensitive scintillation devices, to nanomaterials used in biotechnology, e.g. high-resolution imaging and theranostics. However, consistently, in the design of new photoluminescent solid state materials, it is first of all necessary to adhere to the well-known criteria of molecular engineering to obtain a substance that emits light of a specific colour and to ensure maximum efficiency in the conversion of excitation radiation into emitted one. High-quality phosphor materials, obtained by doping with ions with specific emission properties, require a host crystal structure exhibiting, on the one hand (1) a one-site crystal structure of the host cation substituted by the dopant ion, limiting undesirable energy transfers between energetically unequal the same excited states of ions of the same dopant, (2) characterised by a similar ionic radius to the dopant and thus charge to avoid the need for compensation, and, on the other hand, (3) by the lowest possible phonon energy, limiting the radiationless quenching phenomenon. A class of crystalline hosts that have been gaining much interest, meeting the above criteria for doping with lanthanide ions with excellent thermal properties and high chemical stability, is rare earth orthophosphates

* Corresponding author. Department of Biological, Chemical and Pharmaceutical Sciences and Technologies (STEBICEF), University of Palermo and INSTM UdR – Palermo, Viale delle Scienze, Bld.17, Palermo, I-90128, Italy.
E-mail address: marialuisa.saladino@unipa.it (M.L. Saladino).

https://doi.org/10.1016/j.ceramint.2023.04.159
Received 21 March 2023; Received in revised form 12 April 2023; Accepted 21 April 2023
Available online 23 April 2023

[1–6]. These compounds have the general formula $REPO_4$ where RE = Y, Ln, Gd etc. and can be organised in four different crystalline forms: *Xenotime* ($REPO_4$) with a tetragonal structure (I41/amd) similar to zircon, *Monazite* ($REPO_4$) with a monoclinic structure (P21/n), Rhabdophane ($REPO_4 \bullet 0.8H_2O$) with a hexagonal ($P6_222$) and Churchite ($REPO_4 \bullet 2H_2O$) with monoclinic structure (C2/c) [7,8]. The most interesting among the rare-earth orthophosphates for luminescent applications is YPO_4 for its chemical and thermal stability, for its ability to incorporate dopant ions in high quantities, for its high luminescence yield, and high refractive index [9–14]. Anhydrous YPO_4 is mainly obtained with a tetragonal structure, which is made up of two types of polyhedra, PO_4 tetrahedral, and YO_8 dodecahedral connected to each other through each vertex of the polyhedra. In PO_4 tetrahedra, four O atoms surround the P atom, while in YO_8 polyhedra eight O atoms surround the Y atom. Each oxygen atom connects two Y atoms and an atom of P, while each atom of Y or atom of P connects exclusively oxygen atoms [5].

In contrast to nanosized semiconductor (quantum size-effect) and metallic (plasmonic properties) materials, optical luminescent nanomaterials based on dielectric materials are being developed not to obtain new physical properties, but primarily for their use in specific solutions where the use of ultrafine material particles is beneficial. Examples include their dispersibility in a variety of media allowing them to have specific properties while maintaining their optical transparency (size much smaller than the light wavelength) or their use after appropriate surface functionalization for specific binding to biomaterials (nanotheranostics). For this reason, it is critical to develop methods for their synthesis that enable them to be obtained in a form that is as morphologically homogeneous as possible and at the same time characterised by the lowest possible number of defects associated with their small size. Therefore, at present, many methods have been developed to prepare these materials in nanosize, for example: the sol-gel method allows to prepare spherical particles with variable size from a few tens of nanometers up to a few hundred [15,16]; the precipitation gave irregular spheroidal particles with dimensions between 20 and 80 nm [17,18], solid state reaction gives particles with irregularly shape between 500 nm and 1 μm [19,20], hydrothermal method give needle-shaped particles about 20–40 nm long and about 10 nm wide, or particles with a shape similar to rice grains about 50 nm large [21–24]; combustion produces irregular spherical particles of about 20–50 nm [25]. Microwave assisted synthesis was also used to obtain well-dispersed uniform spheres (~0.7–1.5 μm in diameter) [7,26].

However, the simple and efficient synthesis of YPO_4 nanocrystals having a narrow particle size distribution and uniform morphology remains still an objective to be achieved. This result can be important to properly control and modify the optical properties, since they depend on various factors including the degree of crystallinity, the presence of defects in the lattice, the shape and size of the particles. Zou et al. [27] and Li [28] gave an overview of the YPO_4 features at different conditions in autoclave. Since the hydrothermal synthesis is the most promising for the scale-up and the control of the shape, the goal of this work was to investigate the effect of the time of hydrothermal treatment on the YPO_4:Eu nanophosphors formation, not yet investigated. Eu^{3+} was chosen as a dopant because it emits in the visible range and has a characteristic emission spectrum with narrow and easily recognizable bands. These bands are associated with the two most typical emission transitions: the $^5D_0 \rightarrow {}^7F_2$ hypersensitive transition, associated with the electric dipole whose intensity strongly depends on the local symmetry, and $^5D_0 \rightarrow {}^7F_1$, associated with the magnetic dipole which is negligibly affected by changes in local symmetry. These Eu^{3+} characteristics allow correlating optical properties with structural and morphological features.

2. Experimental part

2.1. Materials

$Y(NO_3)_3 \bullet 6H_2O$ (Aldrich, 99.8%, CAS 1394-98-9); $Eu(NO_3)_3 \bullet 5H_2O$ (Aldrich, 99.9%, CAS 63026-01-7); KH_2PO_4 (Sigma, ≥98.0%, CAS 7778-77-0); KOH (Carlo Erba, 85% min, CAS 1310-58-3); HNO_3 (Aldrich, 70% wt A. C. S. reagent, CAS 7697-37-2); Deionized H_2O (conductibility <1.5 μS/m).

2.2. Synthesis of YPO_4:Eu nano-needles

The synthesis of the YPO_4:Eu nanopowders of nano-needle shape was carried out by phosphate precipitation followed by a hydrothermal treatment in an autoclave. The scheme of the synthesis is reported in Fig. 1.

10 mL of aqueous solutions of KH_2PO_4 (0.2 mol/L), $Y(NO_3)_3 \bullet 6H_2O$ (0.2 mol/L) and of $Eu(NO_3)_3 \bullet 5H_2O$ (0.01 mol/L) were prepared, so that the moles of europium were equal to 5% with respect to the moles of yttrium. The two metal nitrate solutions were stirred using a magnetic stirrer and, once the salts were completely solubilized, were combined together. After that, the solution containing the phosphates was added to the nitrate solution. The formation of a white suspension was rapidly observed according to the following reaction:

$$Y(NO_3)_3\ (aq) + KH_2PO_4\ (aq) \rightarrow YPO_4 \downarrow (s) + KNO_3\ (aq) + 2HNO_3\ (aq)$$

The pH of the suspension, which was initially equal to 1.2, measured by a pH meter (HANNA pH211) was adjusted up to a final pH value of 7, by adding an aqueous solution of 3 mol/L of KOH and a few drops of HNO_3 0.1 mol/L. The suspension thus obtained was brought to a volume equal to 50 mL with deionized water and kept under magnetic stirring for 30 min while continuing to monitor the pH to ensure a constant value of ~7 over time. The suspension was then placed in an autoclave inside a borosilicate glass liner with a maximum capacity of 70 mL, occupying approximately ¾ of the volume in order to comply with the correct safety-loading limit of the autoclave. The temperature range was set, starting from room temperature, according to the ramp 50-100-150-200 °C for various times (2, 4, 6, 8, 12, 18, 24, 32, 48 h) and an autogenous pressure of 10 mbar. The products, obtained following the hydrothermal treatment, were filtered by gravity on a Whatman Schleicher & Schuell 5 paper filter (Cat No 1005 070) with a diameter of 70 mm and porosity of 2.5 μm, and washed several times with deionized water, in order to remove the K^+ and NO_3^- ions which can be adsorbed on the solid precipitate, and place in an oven for 24 h at temperature of 70 °C. The percentage yield falls between 74 and 123% and it is influenced by the autoclave treatment time (Figure SI1 of Support Information, SI). Yields greater than 100% could result from the adsorbed water from the samples, as reported in the literature by Garrido-Hernandez et al. [29]. All the obtained YPO_4:Eu white powders, illuminated with a LED lamp, show the typical emission of the Eu^{3+} ion and visible to the naked eye as red colour light.

Methods of Characterisation. X-ray diffractometry (XRD), Raman Spectroscopy, Fourier transform infrared spectroscopy in attenuated total reflectance (ATR-FTIR), Transmission electron microscopy (TEM) coupled with energy dispersive X-Ray spectroscopy (EDS) and Select Area Diffraction (SAED) techniques were used to evaluate the structural and morphological properties of the powders. The luminescence properties were determined by standard luminescence spectroscopy (emission (PL) and excitation (PLE) spectra) and additionally by luminescence lifetime measurements.

XRD patterns were acquired by a Bruker D8 Advance diffractometer in the Bragg-Brentano geometry using Ni-filtered Cu Kα radiation (λ = 1.54056 Å) in the 2θ range 5–80° with a step of 0.008° and a time for step of 5 s. The phase identification was performed by using the X'pert HighScore® Software. In order to obtain information about phase

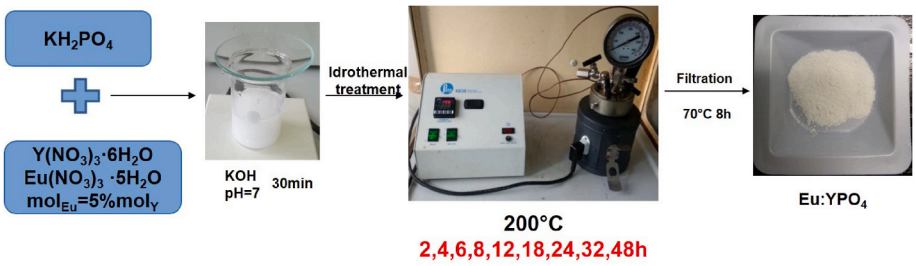

Fig. 1. Scheme of the synthesis of the YPO_4:Eu nanopowders.

composition, the cell parameters and the crystalline size of the phases, the XRD patterns were analysed according to the Rietveld method by using the MAUD software [30,31]. The agreement between the experimental data and the fit was evaluated through the curve of residues and the parameters R_{wp} (<6%), and R_b (<5%).

Raman spectra were acquired in back-scattering geometry by using a Renishaw inVia Raman microscope (equipped with a confocal DM 2500 Leica microscope with length 20x magnification and and thermo-electrically cooled CCD camera as a detector). An argon ion laser (Renishaw plc, Wotton-under-Edge, UK) of wavelength 514 nm (around 9 mW at sample) was used as an excitation source. Each spectrum was accumulated 5 times with exposure time 50 s.

FT-IR ATR spectra were acquired through a VERTEX 70V Bruker spectrophotometer equipped with a Platinum ATR unit with diamond crystal ($\eta = 2.4$) operating in the spectral range between 4000 and 400 cm^{-1}, a spectral resolution of 2 cm^{-1}, and 120 scans. Spectra were acquired at a pressure of 2 hPa. In all spectra a baseline correction of scattering was made. Data analysis was performed using the OPUS 7.5® software.

Scanning Electron Microscopy (SEM). SEM micrographs were acquired using a scanning electron microscope (Nova NanoSEM 450, FEI Company) operating at different voltage values. Specifically, some micrographs were collected using secondary electron detectors (ETD and LTD) at acceleration voltage between 10 and 30 KV, while higher resolution micrographs were collected using the STEM detector (in TEM mode) at 30 KV voltage.

Transmission Electron Microscopy (TEM). TEM micrographs were acquired using the last generation high-resolution scanning/transmission electron (S/TEM) microscope (Thermo Scientific™ Talos™ F200S) equipped with energy dispersive X-Ray spectroscopy (EDS) and operating at 200 kV accelerating voltage. Samples were homogeneously dispersed in bi-distilled water (Millipore) by sonication for 10–15 min. A drop of each suspension was deposited on a copper grid of 200 mesh coated with a transparent polymer (Formvar/carbon) and then dried. Subsequently, specimens were carbonated (Carbon Coater - Balzers CED-010) for TEM investigations.

Photoluminescence emission (PL) and excitation (PLE) spectra were measured using the FLS980 Fluorescence Spectrometer from Edinburgh Instruments. As an excitation source, the 450 W Xenon lamp (for PL and PLE) was used. The R928P side window photomultiplier tube from Hamamatsu was used as a detector. Both the excitation and emission 300 mm focal length monochromators were in Czerny Turner configuration. The excitation arm was supplied with a holographic grating of 1800 lines/mm, blazed at 300 nm, while the emission arm was supplied with ruled grating, 1800 lines/mm blazed at 500 nm. The scanning range was from 250 nm to 680 nm for PLE spectra and from 460 nm to 820 nm for PL spectra. The lifetime measurements were carried out using the same instrument while a 150 W Xe pulsed lamp was used as the excitation source.

3. Results and discussion

3.1. Structure and morphology

The XRD patterns of samples treated at various times are shown in Fig. 2.

As can be seen, the crystallinity of the samples gradually increases with the treatment time. On the contrary, the amorphous fraction decreases with time, as reported by the Rietveld results in Figure SI2 of SI. The XRD patterns of the samples treated between 2 and 8 h show a widening of the XRD peaks which may be due both to the presence of an amorphous phase together with the crystalline phase and to the reduced size of the crystallites, which affects the peak width. The transformation from amorphous to the stable phase tetragonal occurs completely with 12 h of treatment (Figure SI2 of SI). The XRD pattern of the samples treated between 12 and 48 h show very narrow XRD peaks indicative of samples totally crystalline. The XRD patterns showed that the nanopowders are constituted by the tetragonal crystalline phase *Xenotime-(Y)* of yttrium orthophosphate YPO_4 (JCPDS: 00-011-0254). No diffraction peak of any secondary phases was observed. The cell parameters **a** and **c**, obtained for each sample, through Rietveld refinement analysis, are given in Fig. 3.

The cell parameter ***a*** increases as the treatment temperature increases, while the cell parameter ***c*** decreases up to a treatment of 18 h. These results indicate that the time in autoclave influences the crystallite growth by modifying both directions of the lattice and probably the shape of the particles. It is probable that after 12 h a balance will be reached whereby the aforementioned parameters remain constant even for longer treatments.

The Raman and IR spectra of samples treated at various times are shown in Figs. 4a and Fig. 5, and SI3, respectively. Seven of the ten characteristic Raman modes were observed [32]. It can be noted that increasing the treatment time, the observed Raman modes become more distinct and more characteristic of the crystal structure which is confirmed by XRD data. In detail, for the time lower than 6 h, most of the bands are wide and not clearly defined, which is most likely due to structural imperfections. It is worth noting that short processing times are characterised by a significant shift of the corresponding modes compared to the literature data for the crystal structure (Fig. 4b). The most characteristic changes can be observed for the internal modes corresponding to the PO_4 stretching mode with a maximum at 998 cm^{-1}, which becomes sharper with increasing synthesis time. The same situation is observed for the rest of the observed modes. The E_g mode at 1024 cm^{-1} appears only after 12 h. With further processing, it becomes more pronounced. The shoulder with a maximum at around 975 cm^{-1} disappears and is not detected for powders with a synthesis time of more than 24 h. A similar situation was observed when comparing the Raman spectra of powders and bulk structures, and the powders were characterised by an asymmetric broadening of the peak [33]. The presence of a shoulder band at 995 cm^{-1} is associated to the presence of non-integrated Eu^{3+} ions in the YPO_4 matrix.

In detail, the IR peak at about 990 cm^{-1} corresponds to the antisymmetric stretching of the P–O bond, the two peaks at 638 cm^{-1} and

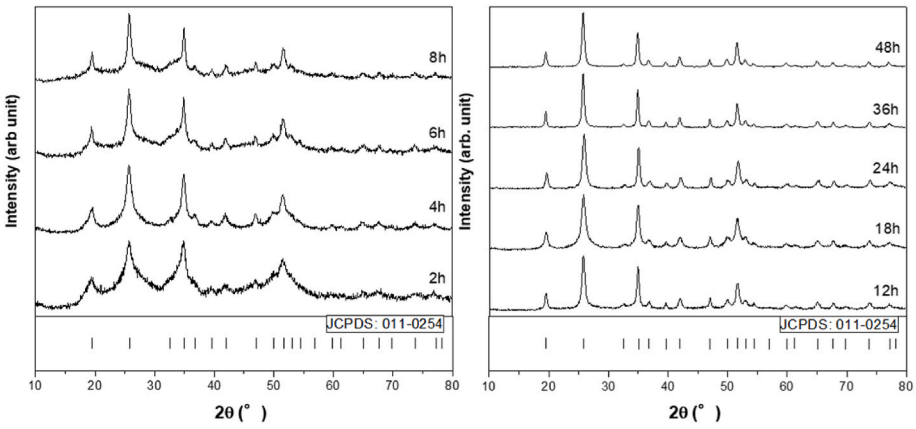

Fig. 2. XRD patterns of YPO_4:Eu samples synthesized at different times.

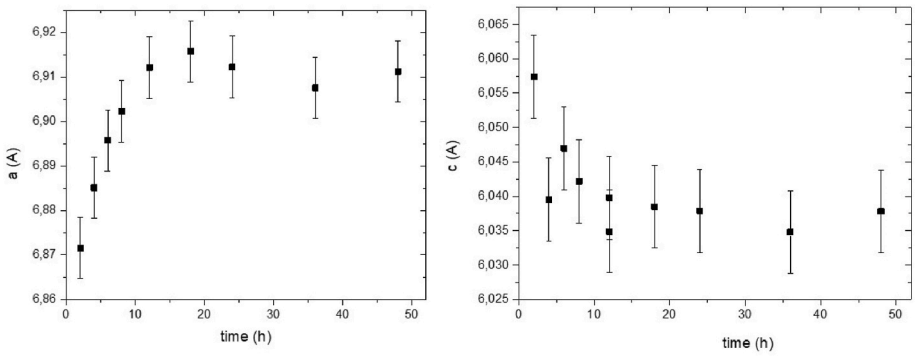

Fig. 3. Cell parameters (**a, c**) of YPO_4:Eu nanopowders at different times of synthesis.

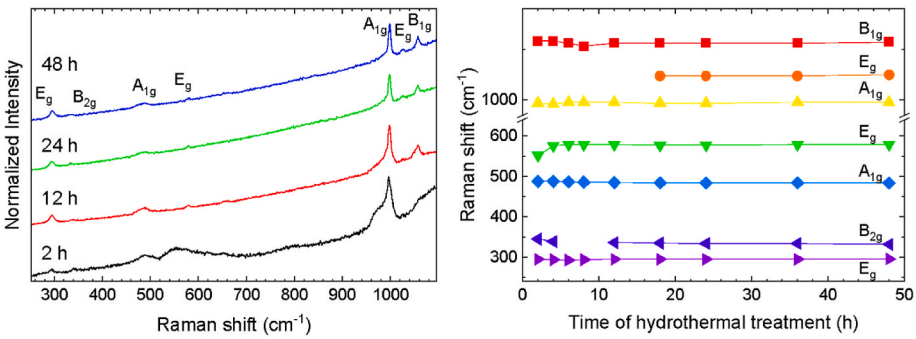

Fig. 4. left) Raman spectra of the YPO_4:Eu nanopowders prepared by hydrothermal synthesis at various treatment times. right) Raman shift as function of the treatment time.

521 cm^{-1} to the antisymmetric bending of the O–P–O and the peak at 430 cm^{-1} to the symmetrical bending of the O–P–O (Fig. 5). A band at 710 cm^{-1} attributable to the stretching of the P–OH group which is found mainly on the surface of the particles can also be observed. In these cases, the splitting of the P–O band is also favoured [34–36].

The stretching at 3200 cm^{-1} and the bending at 1640 cm^{-1} of the O–H groups are evident in the samples treated up to 24 h, while in those at 36 and 48 h these bands are only slightly hinted at, indicating the presence of adsorbed or interstitial water and not of coordination water. Furthermore, the intensity of these signals decreases as the treatment time increases. In addition, the intensity of the asymmetrical stretching and bending bands of the phosphate increases as the treatment time increases, which indicates an increase in the degree of crystallinity, in accordance with XRD data. No significant shift is observed. A doubling of the band relating to the asymmetrical stretching of the P–O bond is observed with the time increasing, due to the water content decreasing, which influences the band shape, the crystallinity and decreases defects.

It can therefore be stated that the precipitate treated in autoclave progressively evolves from an amorphous system to the tetragonal crystalline phase of yttrium phosphate and that during this process there is also the gradual loss of adsorbed water. This mechanism explains why the samples treated between 2 and 8 h show a yield greater than 100% (see previous paragraph and Figure SI2 of SI), which decreases as the treatment time increases and falls below 100% only after 12 h, time for which only the crystalline phase is obtained. In addition, the presence of OH- ions on the particle surface acts as a quencher to the luminescence intensity which can be significantly enhanced after removing OH- ions by a heat treatment (discussed in the paragraph 3.2).

The morphology and particle size of samples obtained by the hydrothermal method were investigated both by SEM and TEM analyses.

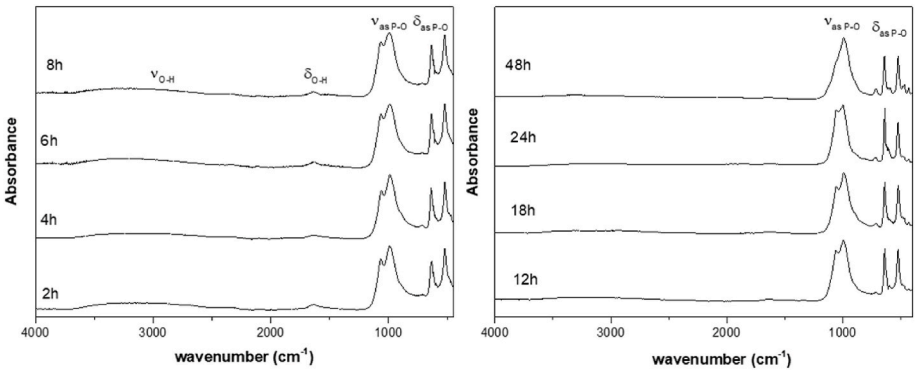

Fig. 5. ATR-FTIR spectra of the YPO_4:Eu nanopowders at different treatment times.

From the SEM micrographs it is clearly observable that the nanopowders obtained after 8 h and 18 h are made up of aggregates in needle-like clusters, while those obtained after 48 h are aggregates in spheroidal clusters (Figure SI4 in SI).

Some representative TEM micrographs with different magnification of the YPO_4:Eu nanopowders obtained after 8, 18 and 48 h are reported in Fig. 6. The relative histograms of distribution of the observed particle sizes are reported in Figures SI5-SI7 of SI. The YPO_4:Eu nanopowders obtained **after 8 h** of treatment are constituted by nanoparticles having a so-called rod shape whose average size is about 42 nm in length and 11 nm in thickness, in accordance with the morphology reported by Wu et al. [37] which obtained similar YPO_4:Nd particles by hydrothermal synthesis at pH = 6, 180 °C for 24 h. The YPO_4:Eu nanopowders obtained **after 18 h** are constituted by nanoparticles having a rod shape whose average size is about 38 nm in length and 12 nm in thickness, in accordance with the morphology reported in the literature [37]. The YPO_4:Eu nanopowders obtained **after 48 h** are constituted by nanoparticles with a so-called rice scar shape whose average size is about 24 nm in length and 14 nm in thickness, in accordance with the morphology reported in Vanetsev et al. [7], which obtained similar particles of YPO_4 by microwave-assisted hydrothermal synthesis at pH = 9 after 4 h of treatment. The EDS spectra (not reported) acquired on the particles show the presence of yttrium, phosphorus, oxygen, europium and potassium at the maps of elements (Figure SI9 of SI) indicate that these elements are homogeneously distributed in the particles and that there is no segregation of the dopant. Potassium comes from the reagent KH_2PO_4. SAED patterns acquired on these particles indicate that the particles have a crystalline structure with a spacing between planes corresponding, in both images, to 2.7 Å of the (211) plane of the *Xenotime-* (Y) tetragonal phase (Figures SI9 and SI10 of SI).

It is known that for the properties of luminescent nanocrystals, an important material feature is their surface-to-volume ratio (S/V), which gives some idea of the number of surface defects and dopant ions near the surface, which can be quenched much faster than ions in the crystallographically well-defined 'volume' part of the nanocrystal. For this purpose, assuming a cylindrical shape observed using TEM, the S/V was calculated as follows: 0.44 for 8 h, 0.32 for 18 h and 0.37 for 48 h. From these results, it can be seen that first, between 8 and 18 h, there is a clear decrease in S/V of 30% and then, between 18 and 48 h, a relatively small increase of around 16%.

3.2. Photoluminescence

In order to correlate the crystal structure parameters and the morphology of the samples obtained at different times of treatment with the local structure of the dopant ions, which have a fundamental influence on their luminescence properties, selective studies by optical spectroscopy were carried out. PLE and PL spectra, recorded at room temperature, are reported in Fig. 7 and in Figure SI11 of SI.

From the excitation spectrum we observed narrow peaks assigned to the intra-4f transitions of the Eu^{3+} from the $^7F_0$ ground level (and populated at room temperature $^7F_1$ level) [38,39]. Since the transition $^7F_{0,1} \rightarrow {}^5L_6$ has a greater intensity than the others, the emission spectrum was recorded by excitation at 396 nm. In the emission spectrum, the characteristic bands of the Eu^{3+} ion are observed in the orange-red region relating to the transitions $^5D_0 \rightarrow {}^7F_J$ (where J = 1, 2, 3, 4).

No shift in the positions of the bands is observed between the nanopowders obtained at different conditions. As shown above, the morphology of the crystallites is reflected in the change of the determined lattice parameters, with the parameter ***a*** initially increasing strongly while ***c*** decreases as the length is shortened and the cross-section increases. An additional factor that can quench the luminescence is also the presence of hydroxyl groups, visible in IR spectra up to the synthesis time of 8 h and whose absorption visibly disappears after 12 h. In order to see how these changes affect the local surroundings of the dopant ions, the specific properties of the emission transitions of Eu^{3+} ions associated with the electric dipole (transition $^5D_0 \rightarrow {}^7F_2$) and the magnetic dipole ($^5D_0 \rightarrow {}^7F_1$) were used. As it is well known, their intensity ratio, calculated by integrating the areas of the corresponding bands, also known as the asymmetry ratio (or simply R-factor), is a

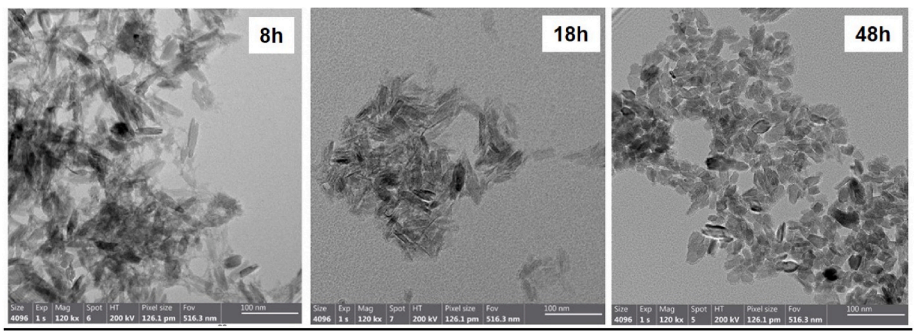

Fig. 6. TEM micrographs of YPO_4:Eu nanopowders synthesized for 8, 18 and 48 h in autoclave.

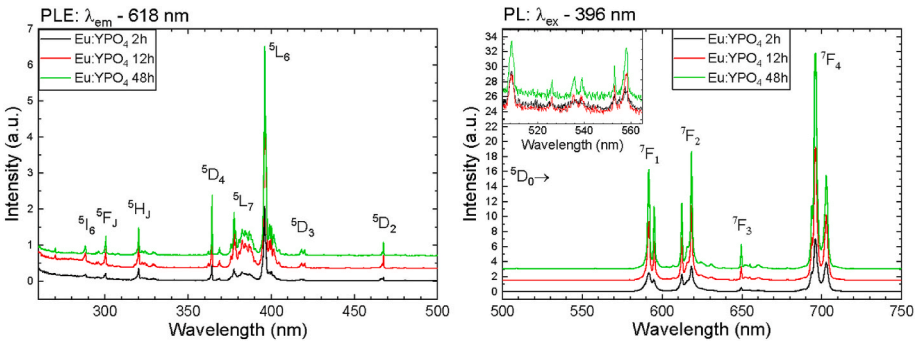

Fig. 7. PLE and PL spectra of the YPO_4:Eu nanopowders.

measure of the local symmetry of the Eu^{3+} ion, taking values from below one for systems with very high symmetry to as much as ten times higher for systems characterised by very low symmetry (including glassy materials). In the case studied here, it can be used to determine the degree of disorder in the surroundings of ions located in the near-surface zone of grains, whose concentration relative to bulk ions depends directly on the size of the nanocrystallites.

From the dependence of the R factor on the synthesis time, shown in Fig. 8, it can be seen that its course corresponds with the S/V value determined for the selected samples, first, already after 12 h we observed its rapid decrease and then only slight changes between 18 and 48 h. This relationship should be further interpreted in the context of the results of IR data, which additionally indicated the presence of hydroxyl groups in the sample obtained in the 12 h synthesis, further influencing the structural ordering of the YPO_4 structure and whose elimination in this range is associated precisely with the 'closing' of the surface and a reduction in the S/V value.

These results are also reflected in the luminescence decay measurements shown in Fig. 9a. As can be seen, essentially all decays except for the sample obtained at the shortest synthesis times, in particular 2 h, are characterized by a single-exponential decay, confirming a single site of the Eu^{3+} ion in the YPO_4 crystal lattice. The non-exponential decay for the samples with the shortest synthesis times, resulting also in the shortest fitted luminescence lifetimes (Fig. 9b), is due to disorder in its closest surroundings resulting most likely from the presence for these samples of hydroxyl groups and additionally from the dopant surface sites, favouring the formation of structural defects in their closest surroundings and consequently the growth of non-radiative transitions. This is also confirmed by the fact that the highest S/V ratio is characterised by samples obtained below 8 h, then for 12 and 18 h there is a significant decrease in the S/V ratio and a simultaneous decrease in the content of OH^- groups. It can also be seen that in the case of samples obtained in synthesis of more than 18 h, for which changes in particle morphology resulting already in a slight increase in S/V ratio are observed between 18 and 48 h, such significant changes in the values of lifetimes as for shorter synthesized samples are no longer observed. This indicates that the radiative processes of excited Eu^{3+} ions are much more influenced by the presence of hydroxyl groups and associated "bulk" defects compared to near-surface defects. We proved once more that the shape of particles can influence the distance between Eu^{3+} ions in the phosphor, which affect the fluorescence lifetime or the energy transfer [40–42].

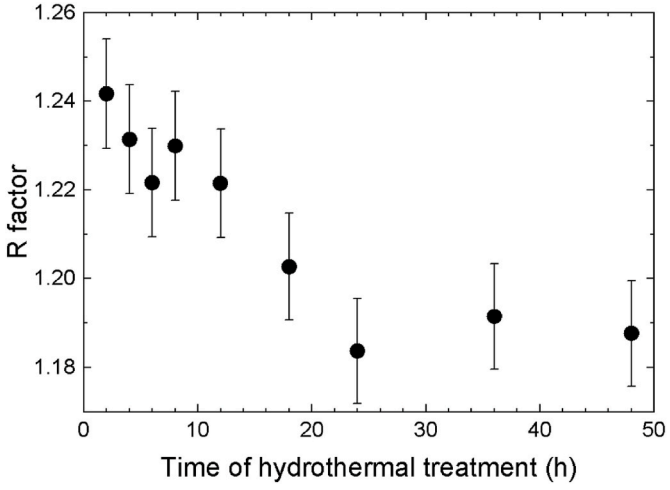

Fig. 8. Asymmetry ratio $R = I_{int.}$ ($^5D_0 \rightarrow {}^7F_2$)/$I_{int.}$ ($^5D_0 \rightarrow {}^7F_1$) as a function of hydrothermal treatment time.

4. Conclusions

The precipitation followed by a hydrothermal treatment in an autoclave allows to obtain YPO_4:Eu nanoparticles with *Xenotype* structure exhibiting typical intense emission in the red spectral region upon UV excitation. The precipitate treated in an autoclave progressively evolves from an amorphous system to the tetragonal crystalline phase of yttrium phosphate with the time of treatment. During this process there is also the gradual loss of adsorbed water. The first of main results of this study concerns the definition of the minimum time of treatment necessary to obtain a totally crystalline sample (12 h). Lower time of treatments gave hydrated powders containing an amorphous part together with the crystalline phase. On the other hand, it was demonstrated that a time of treatment >8 h modifies the shape and size of particles from nano-needle to -rice shape, which changes the S/V (surface to volume) ratio first significantly decreasing it compared to samples obtained at the shortest synthesis times and above 18 slightly increasing it already. It is shown that the asymmetric R-factor defined as a ratio of $^5D_0 \rightarrow {}^7F_2$ and $^5D_0 \rightarrow {}^7F_2$ emission transitions, commonly used for determination of changes in local symmetry of the Eu^{3+} ion, depends on the synthesis time and corresponds to the S/V value of the samples and is thus related to the disordered near-surface states of the Eu^{3+} ions. Analysis of the IR spectrum and the corresponding luminescence characteristics showed that the disappearance of the presence of hydroxyl groups in the sample obtained at 12 h and longer synthesis affects the structural ordering of the YPO_4 structure. Luminescence decay measurements confirm a single site of the Eu^{3+} ion in the YPO_4 crystal lattice, and the non-exponential decay observed for shorter synthesis times is explained by the disorder in the surroundings caused by hydroxyl groups and dopant surface sites. The radiative processes of excited Eu^{3+} ions were found to be relatively more influenced by hydroxyl groups and volume defects than by surface defects.

The obtained results allow, in the future, to prepare by a simple and scalable hydrothermal method luminescent RE-doped YPO_4 nanopowders with a morphology that will enable their optimal application, for example, in the synthesis of glass-ceramics, nanocomposites or simply as highly dispersive colloidal powders.

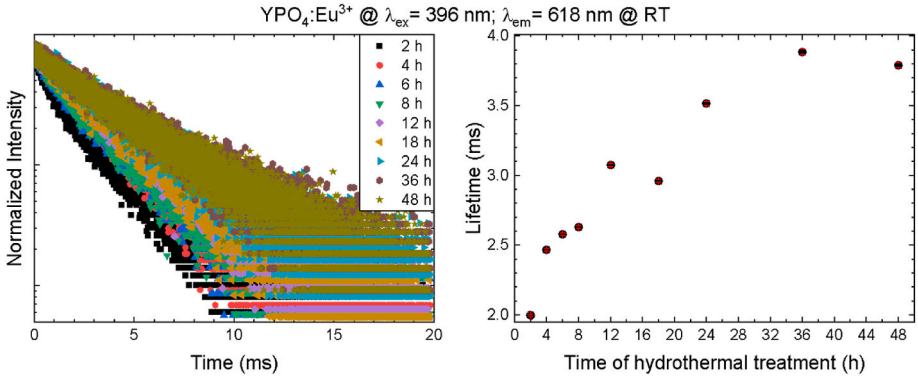

Fig. 9. Luminescence lifetime for samples obtained at different synthesis times (a) and determined lifetimes from single-exponential fitting (b).

Funding

F.A thanks MIUR for the Project PON Ricerca e Innovazione 2014-2020 – Avviso DD 407/2018 "AIM Attrazione e Mobilità Internazionale" (AIM1808223).

Author contributions

MLS and DH: Conceptualization and methodology, writing–review and editing. LB: Synthesis. FA: XRD patterns and FT-IR spectra. CM and CL: SEM and TEM investigation. VB: optical properties (PL and PLE spectra) and Raman spectra. All authors contributed to the article and approved the submitted version.

Data availability statement

The datasets generated during and/or analysed during the current study are available from the corresponding author on reasonable request.

Declaration of competing interest

The authors declare that they have no known competing financial interests or personal relationships that could have appeared to influence the work reported in this paper.

Appendix A. Supplementary data

Supplementary data to this article can be found online at https://doi.org/10.1016/j.ceramint.2023.04.159.

References

[1] E. Khouri, M. Elaatmani, G. Della Ventura, A. Sodo, R. Rizzi, M. Rossi, F. Capitelli, Synthesis, structure refinement and vibrational spectroscopy of new rare-earth tricalcium phosphates $Ca_9RE(PO_4)_7$ (RE = La, Pr, Nd, Eu, Gd, Dy, Tm, Yb) Ceramics, International 43 (2017) 15645–15653, https://doi.org/10.1016/j.ceramint.2017.08.121.

[2] L. Zhang, H. Jiu, Y. Fu, Y. Sun, Y. Wang, Preparation and photoluminescence enhancement of Li^+ and Eu^{3+} co-doped YPO_4 hollow microspheres, J. Rare Earths 31 (2013) 449–455.

[3] H. Lai, A. Bao, Y. Yang, W. Xu, Y. Tao, H. Yang, Preparation and luminescence property of Dy^{3+}doped YPO_4 phosphors, J. Lumin. 128 (2008) 521–524.

[4] T. Subramani, M. Ruwaid Rafiuddin, A. Shelyug, S. Ushakov, A. Mesbah, Synthesis, crystal structure, and enthalpies of formation of churchite-type $REPO_4{\cdot}2H_2O$ (RE = Gd to Lu) materials, Crystal Growth & Design, American Chemical Society 19 (8) (2019) 4641–4649.

[5] J. Han, Y. Wang, R. Liu, Theoretical and experimental investigation of Xenotime-type rare earth phosphate $REPO_4$, (RE = Lu, Yb, Er, Y and Sc) for potential environmental barrier coating applications, Sci. Rep. 10 (2020), 13681.

[6] J. Huang, R. Gao, Z. Lu, D. Qian, W. Li, B. Huang, X. He, Sol–gel preparation and photoluminescence enhancement of Li^+ and Eu^{3+} co-doped YPO_4 nanophosphors, Opt. Mater. 32 (2010) 857–861.

[7] A.S. Vanetsev, E.V. Samsonova, O.M. Gaitko, K. Keevend, A.V. Popov, U. Mäeorg, H. Mändar, I. Sildos, YuV. Orlovskii, Phase composition and morphology of nanoparticles of yttrium orthophosphates synthesized by microwave-hydrothermal treatment: the influence of synthetic conditions, J. Alloys Compd. 639 (2015) 415–421.

[8] N. Clavier, A. Mesbah, S. Szenknect, N. Dacheux, Monazite, rhabdophane, xenotime & churchite: vibrational spectroscopy of gadolinium phosphate polymorphs, Spectrochim. Acta Mol. Biomol. Spectrosc. 205 (2018) 85–94.

[9] M. Srivastava, L. Sanatombi Devi, R. Josh, B. Pratap Singh, R. Singh Ningthoujam, Effect of signal to noise ratio on luminescence property of YPO_4:Eu, Mater. Lett. X 16 (2022), 100170, https://doi.org/10.1016/j.mlblux.2022.100170.

[10] D.A. Mikhaylov, E.A. Potanina, A.V. Nokhrin, A.I. Orlova, P.A. Yunin, N. V. Sakharov, M.S. Boldin, O.A. Belkin, V.A. Skuratov, A.T. Issatov, V. N. Chuvil'deev, N.Y. Tabachkova, Investigation of the microstructure of fine-grained YPO4:Gd ceramics with xenotime structure after Xe irradiation, Ceramics 5 (2) (2022) 237–252, https://doi.org/10.3390/ceramics5020019.

[11] Y. Che, S. Sun, J. Lu, F. Zheng, G. Yu, Y. Cao, L. Wang, L. Sun, Y. Yin, Z. Wang, D. Zhong, B. Teng, Preparation and systematic spectra analysis of YPO_4 crystal co-doped with Er^{3+} and Yb^{3+}, J. Lumin. 248 (2022), 118957 https://doi.org/10.1016/j.jlumin.2022.118957.

[12] K. Maciejewska, L. Marciniak, Influence of the synthesis conditions on the morphology and thermometric properties of the lifetime-based luminescent thermometers in YPO_4:Yb^{3+},Nd^{3+} nanocrystals, ACS Omega 7 (35) (2022) 31466–31473, https://doi.org/10.1021/acsomega.2c03990.

[13] J. Kappelhoff, J.-N. Keil, M. Kirm, V.N. Makhov, K. Chernenko, S. Möller, T. Jüstel, Spectroscopic studies on Pr^{3+} doped YPO_4 and $LuPO_4$ upon vacuum ultraviolet (VUV) and synchrotron radiation excitation, Chem. Phys. 562 (2022), 111646, https://doi.org/10.1016/j.chemphys.2022.111646.

[14] J. Cho, Deciphering competing radiative relaxation pathways observed in Pr^{3+}-Activated yttrium-based compounds: UV emission versus visible emission, J. Lumin. 253 (2023), 119460, https://doi.org/10.1016/j.jlumin.2022.119460.

[15] B. Kahouadji, L. Guerbous, D.J. Jovanović, M.D. Dramićanin, M. Samah, L. Lamiri, L. Benchallal, M.M. Cincović, Annealing effect on the photoluminescence properties of Ce^{3+} doped YPO_4 nanophosphors, Opt. Mater. 91 (2019) 35–41.

[16] B. Kahouadji, L. Guerbous, A. Boukerika, Slobodan D. Dolić, Dragana J. Jovanović, Miroslav D. Dramićanin, Sol gel synthesis and pH effect on the luminescent and structural properties of YPO_4:Pr^{3+} nanophosphors, Opt. Mater. 70 (2017) 138–143.

[17] X. Li, H. Wang, L. Guan, Y. Fu, Z. Guo, K. Yuan, L. Tie, Z. Yang, F. Teng, Influence of pH Value on Properties of YPO_4:Tb^{3+} phosphor by co-precipitation method, J. Rare Earths 33 (2015) 346–349.

[18] Y. He, M. Zhao, Y. Song, G. Zhao, X. Ai, Effect of Bi^{3+} on fluorescence properties of YPO_4:Dy^{3+} phosphors synthesized by a modified chemical co-precipitation method, J. Lumin. 131 (6) (2011) 1144–1148.

[19] Z. Yahiaoui, M.A. Hassairi, M. Dammak, Synthesis and optical spectroscopy of YPO_4:Eu^{3+}Orange–red phosphors, J. Electron. Mater. 46 (2017) 4765–4773.

[20] T. Deng, S. Yan, J. Hu, A novel narrow band UV-B emitting phosphor-YPO4:Sb^{3+}, Gd^{3+}, J. Rare Earths 34 (2016) 137–142.

[21] Q. Liu, Y. Su, H. Yu, W. Han, YPO_4 nanocrystals: preparation and size-induced lattice symmetry enhancement, J. Rare Earths 26 (2008) 495–500.

[22] F. Armetta, V. Boiko, D. Hreniak, R.C. Ponterio, M.L. Saladino, Luminescent YPO4 : Eu@PVA Dispersions for Anti-counterfeiting Ink Applications, Mat. Lett. (2023), 133653, https://doi.org/10.1016/j.matlet.2022.133653.

[23] G. Wang, L. Gao, H. Zhu, et al., Hydrothermal synthesis of blue-emitting YPO_4:Yb^{3+} nanophosphor, Front. Mater. Sci. 10 (2016) 197–202.

[24] J. Wu, M. Li, H. Jia, Z. Liu, Hengjun Jia, Controllable preparation and fluorescence property of spherical nano-phosphor YPO_4:Eu^{3+}, J. Lumin. 225 (2020), 117367.

[25] S. Liu, Z. Xiu, F. Xu, W. Yu, J. Yu, G. Feng, Combustion synthesis and photoluminescence of Nd^{3+}-doped YPO_4 nanocrystals, J. Alloys Compd. 459 (2008) 407–409.

[26] Q. Zhu, Z. Xu, Z. Wang, X. Wang, X. Li, X. Sun, Ji-G. Li, Multi-color emission in monodispersed spheres of tetragonal yttrium phosphate: microwave-assisted fast synthesis, formation mechanism, temperature-dependent luminescence, and application in anti-fake labeling, CrystEngComm 20 (2018) 3187–3201, https://doi.org/10.1039/C8CE00365C.

[27] J. Zou, Q. Zhu, X. Li, X. Sun, Ji-Guang Li, Controlled hydrothermal processing of multiform (Y0.95Eu0.05)PO_4 crystals and comparison of photoluminescence, J. Alloys Compd. 870 (2021), 159380, https://doi.org/10.1016/j.jallcom.2021.159380.
[28] P. Li, Y. Zhang, L. Zhang, F. Li, Y. Guo, Y. Li, W. Gao, Phase control of Eu^{3+}-doped YPO_4 nano-/microcrystals, Cryst. Growth Des. 17 (11) (2017) 5935–5944, https://doi.org/10.1021/acs.cgd.7b01038.
[29] A. Garrido-Hernandez, Synthesis by Hydrothermal Process of Lanthanide Orthophosphates for Optical Applications, Other. Université Blaise Pascal - Clermont-Ferrand II, 2015. NNT:2015CLF2256.
[30] R.A. Young (Ed.), University Press, Oxford, 1993, p. 298.
[31] L. Lutterotti, S. Gialanella, Acta Mater. 46 (1) (1998) 101–110.
[32] E. Stavrou, et al., J. Phys.: Conf. Ser. 121 (2008), 042016, https://doi.org/10.1088/1742-6596/121/4/042016.
[33] A.K. Gulnar, V. Sudarsan, R. Kumar Vatsa, T. Sakuntala, A. Kumar Tyagi, U. Kumar Gautam, A. Vinu, Nucleation sequence on the cation exchange process between Y0.95Eu0.05PO4 and CePO4 nanorods, Nanoscale 2 (2010) 2847–2854, https://doi.org/10.1039/c0nr00334d.
[34] A. Garrido-Hernandez, Synthesis by Hydrothermal Process of Lanthanide Orthophosphates for Optical Applications, Other. Université Blaise Pascal - Clermont-Ferrand II, 2015. NNT:2015CLF2256.
[35] N.K. Nguyen, M. Leoni, D. Maniglio, C. Migliaresi, Hydroxyapatite nanorods: soft-template synthesis, characterization and preliminary in vitro tests, J. Biomater. Appl. 28 (2012) 49–61.
[36] K. Nakamoto (Ed.), Infrared Spectra of Inorganic and Coordination Compounds, Part A: Theory and Applications in Inorganic Chemistry, sixth ed., Wiley-Interscience, New York, NY, 1986, 9780471743392.
[37] Y. Wu, Z. Zhang, H. Suo, X. Zhao, C. Guo, 808 nm light triggered up-conversion optical nano-thermometer YPO_4:Nd^{3+}/Yb^{3+}/Er^{3+} based on FIR technology, J. Lumin. 214 (2019), 116578.
[38] S. Hachani, B. Moine, A. El-akrmi, M. Ferid M, Luminescent Properties of some ortho and pentaphosphates doped with Gd^{3+}-Eu^{3+}: potential phosphors for vacuum ultraviolet excitation, Opt. Mater. 31 (2009) 678–684.
[39] S. Hachani, B. Moine, A. El-akrmi, M. Ferid M, Energy transfers between Sm^{3+} and Eu^{3+} in YPO_4, LaP_5O_{14} and LaP_3O_9 phosphates. Potential quantum cutters for red emitting phosphors, J. Lumin. 130 (2010) 1774–1783.
[40] L. Liu, J. Li, J. Liu, Z. Yu, R. Pang, C. Li, J. Mater. Sci. Mater. Electron. 31 (2020) 19159–19167.
[41] P. Borovik, V. Oestreicher, P.C. Angelomé, B.C. Barja, M. Jobbágy, J. Sol. Gel Sci. Technol. 102 (2022) 279–287.
[42] E. Chaudan, J. Kim, S. Tusseau-Nenez, P. Goldner, O.L. Malta, J. Peretti, T. Gacoin, J. Am. Chem. Soc. 140 (30) (2018) 9512–9517.